

RESEARCH PAPER

Transcript and protein profiling analysis of OTA-induced cell death reveals the regulation of the toxicity response process in *Arabidopsis thaliana*

Yan Wang^{1,*}, Xiaoli Peng^{1,*}, Wentao Xu^{1,2,†}, YunBo Luo^{1,2}, Weiwei Zhao¹, Junran Hao¹, Zhihong Liang², Yu Zhang² and Kunlun Huang^{1,2,†}

¹ Laboratory of food safety and molecular biology, College of Food Science and Nutritional Engineering, China Agricultural University, Beijing 100083, PR China

² The Supervision, Inspection & Testing Center of Genetically Modified Organisms, Ministry of Agriculture, Beijing 100083, PR China

* These authors contributed equally to this work.

† To whom correspondence should be addressed. E-mail: hk1009@163.com or xuwentao@sina.com

Received 13 October 2011; Revised 13 December 2011; Accepted 13 December 2011

Abstract

Ochratoxin A (OTA) is a toxic isocoumarin derivative produced by various species of mould which mainly grow on grain, coffee, and nuts. Recent studies have suggested that OTA induces cell death in plants. To investigate possible mechanisms of OTA phytotoxicity, both digital gene expression (DGE) transcriptomic and two-dimensional electrophoresis proteomic analyses were used, through which 3118 genes and 23 proteins were identified as being up- or down-regulated at least 2-fold in *Arabidopsis* leaf in response to OTA treatment. First, exposure of excised *Arabidopsis thaliana* leaves to OTA rapidly causes the hypersensitive response, significantly accelerates the increase of reactive oxygen species and malondialdehyde, and enhances antioxidant enzyme defence responses and xenobiotic detoxification. Secondly, OTA stimulation causes dynamic changes in transcription factors and activates the membrane transport system dramatically. Thirdly, a concomitant persistence of compromised photosynthesis and photorespiration is indicative of a metabolic shift from a highly active to a weak state. Finally, the data revealed that ethylene, salicylic acid, jasmonic acid, and mitogen-activated protein kinase signalling molecules mediate the process of toxicity caused by OTA. Profiling analyses on *Arabidopsis* in response to OTA will provide new insights into signalling transduction that modulates the OTA phytotoxicity mechanism, facilitate mapping of regulatory networks, and extend the ability to improve OTA tolerance in *Arabidopsis*.

Key words: Cell death, OTA, proteomic, toxicity response, transcriptomic.

Introduction

In plant pathology, many secondary metabolites produced by fungi are pathogenicity or virulence factors (i.e. they play a role in causing or exacerbating plant disease; Bennett, 2003). Necrotrophic phytopathogenic fungi synthesize a wide range of phytotoxic compounds, including the sphinganine analogue mycotoxins, which are produced by at least two unrelated groups of fungi, *Alternaria* and *Fusarium* spp. AAL toxins and fumonisins (including FB1) are sphinganine analogue mycotoxins that may play a role in virulence (Stone *et al.*, 2000; Egusa *et al.*, 2009). These

toxins inhibit ceramide synthase, resulting in the depletion of ceramides and accumulation of free sphingoid bases. Ultimately, they induce apoptotic (or apoptotic-like) cell death in susceptible tomato cells and mammalian cells (Egusa *et al.*, 2009; Ciacci-Zanella and Jones, 1999).

Ochratoxin A (OTA) is another naturally occurring mycotoxin produced by fungi that is found in a variety of food commodities, such as cereals, green coffee, cocoa, dried fruits, and meat products, resulting in continuous exposure of the human population to OTA (Zhang *et al.*,

2009). OTA has been shown to be nephrotoxic, hepatotoxic, teratogenic, and immunotoxic to several species of animals and is known to cause kidney and liver tumours in mice and rats (Ringot *et al.*, 2006). Several major mechanisms have been shown to be involved in the toxicity of OTA: inhibition of protein synthesis, interference with metabolic systems involving phenylalanine, promotion of membrane lipid peroxidation, disruption of calcium homeostasis, inhibition of mitochondrial respiration, and DNA damage (Ringot *et al.*, 2006). Recent research has focused on the ability of OTA to disturb cellular signalling and regulation, as well as to modulate physiological signals, known to influence cell viability and proliferation. Recent studies have specifically focused on (i) metabolism-mediated toxicity via oxidative stress; (ii) intracellular OTA accumulation as a function of organic anion transporters; and (iii) inter- and intracellular signal transduction at nanomolar concentrations (Boesch-Saadatmandi *et al.*, 2008; Zhang *et al.*, 2009; Malekinejad *et al.*, 2011).

Studies have shown that OTA is produced by phytopathogenic *Aspergillus ochraceus* and *Aspergillus carbonarius* strains, suggesting that this toxin may play a role in the aetiology of plant diseases (Xu *et al.*, 2009). The plant response to attempted infection by microbial pathogens is often accompanied by rapid cell death in and around the initial infection site, a reaction known as the hypersensitive response (HR). Xenobiotics could also induce HR-like lesions. The cellular defence responses involved in induced resistance are either activated directly or primed for augmented expression upon pathogen attack or xenobiotic exposure (Hulten *et al.*, 2006). Many of the cell death regulators that have been characterized in humans, worms, and flies are absent from the *Arabidopsis* genome, indicating that plants probably use other regulators to control this process (Lam *et al.*, 2001). The cell death response in plants is under strict genetic control, as evidenced by the existence of mutants that spontaneously form HR-like lesions (lesion-mimic mutants, *At psi2* and *Cat1AS*) in many plant species, associated with the induction of other components of the plants' defence arsenal, including accumulation of reactive oxygen species (ROS), expression of pathogenesis-related (PR) genes, production of phytoalexin, and the reinforcement of cell walls (Stone *et al.*, 2000). In the presence of OTA, the growth of *Arabidopsis thaliana* on media was significantly inhibited; in addition, cell death was observed with features resembling the HR-type lesions in excised leaves that were infiltrated with this toxin. There was also evidence that cell death was induced by OTA, such as the occurrence of an oxidative burst and the deposition of callose and phenolic compounds (autofluorescence) (Peng *et al.*, 2010).

Although the role of toxins as effectors of disease susceptibility has been well characterized, there is little knowledge about the mechanisms of general or basal resistance of plants to toxins. To understand more about the process by which OTA disturbs cellular signalling and regulation and modulates physiological signals, a genome-wide coverage method was used that allowed identification

of a group of early regulated genes, including transcription factors, that are potentially involved in the transcriptional reprogramming observed during the later stages and in the regulation of the cell death process. By comparing transcript and protein patterns, protein expression driven directly by transcript abundance can be distinguished from that regulated post-transcriptionally.

Here, an expansive view of the early stage of OTA-induced cell death and the regulation of the toxicity response process in *A. thaliana* is reported from an integrated bioinformatics analysis of proteomic and transcriptomic data sets. It was found that (i) a number of xenobiotic and ROS-inducible genes were also up-regulated; (ii) antioxidant enzyme defence responses were enhanced; (iii) photosynthesis and photorespiration were compromised; and (iv) the biological membrane played a relatively large role in transport. Genes and proteins involved in important functional organs and key metabolic pathways are required for the regulation of cell death; therefore, this study brings new insights into the regulation of the toxicity response to OTA in *Arabidopsis*.

Materials and methods

Chemicals

OTA was extracted and purified as described previously (Peng *et al.*, 2010). All other chemicals were of high purity grade.

Plant materials and OTA treatments

Arabidopsis Col-0 wild-type plants were germinated on Murashige and Skoog (MS) medium containing 2% sucrose and 0.8% Phytagar after a 3 d vernalization period at 4 °C under the following conditions: 16 h light/8 h dark period, photosynthetic photon flux density 100 $\mu\text{mol m}^{-2} \text{s}^{-1}$, 22 °C, and 60% relative humidity. Seven-day-old seedlings were planted into soil. Four-week-old plants were used for the experiments.

Briefly, OTA (2 mM and 1 mM) was infiltrated into leaves using a syringe without a needle, as described previously (Gechev *et al.*, 2004). Methanol-infiltrated plants served as controls. Excised leaves were incubated in Petri dishes containing OTA or the corresponding concentration of solvent (methanol) used as a control (Peng *et al.*, 2010) under continuous light or dark at room temperature (22 °C). Samples were taken after 3, 8, 16, 24, 48, and 72 h of treatment.

Chlorophyll content measurement

Chlorophyll content was measured after extraction with hot ethanol, as described by Anderson and Rowan (1965). Leaf tissues (0.2 g fresh weight) were ground and then homogenized in 5 ml of acetone, and they were then placed in the dark for 1 h at room temperature. Extracts were filtered, and the liquid supernatants were measured by the UV-Vis method.

Measurement of the relative leakage rate

Cell death was also determined by electrolyte leakage from the leaves (i.e. the increased conductivity) according to the method of Peng *et al.* (2010). To avoid differences in the ion balance due to the treatment, the results were expressed as relative conductivity rather than absolute conductivity.

Transmission electron microscopy

For electron microscopy, the treated leaves were cut into 2 mm×2 mm pieces and fixed in a 3% glutaraldehyde–0.1 M pH 7.2 phosphate-buffered saline (PBS) solution at room temperature for 3 h. Samples were post-fixed in 1% osmium tetroxide in 50 mM pH 7.2 sodium cacodylate, dehydrated in a graded ethanol series, and embedded in Spur's resin. Blocks were cut with a diamond knife on an LKB-8000 Ultracut ultramicrotome to obtain ultrathin sections, which were stained with 2% uranyl acetate and lead citrate and then examined using a JEM-1230 transmission electron microscope (JEOL, Japan).

RNA extraction

Total RNAs were prepared using an RNeasy pure Plant kit (Qiagen Inc.) according to the manufacturer's instructions. They were subsequently purified using an RNeasy RNA purification kit (Qiagen, <http://www.qiagen.com/>) with on-column DNase digestion. Equal loading was verified by ethidium bromide staining of the gel.

Real-time RT-PCR

For quantitative RT-PCR analysis, leaves were infiltrated as above and samples were collected 3, 8, or 24 h later. Total RNA was isolated as above. The quality of the RNA was assessed with Lab-on-chip analysis using a 2100 Bioanalyzer (Agilent, <http://www.agilent.com/>). cDNA was synthesized using a first-strand cDNA Quantscript RT kit (Tiangen Inc.) according to the manufacturer's instructions. Real-time PCR experiments were performed in triplicate in 25 µl volumes using RealMasterMix (SYBR green) (Tiangen Inc.) in an ABI 7500 Real-time PCR machine (Applied Biosystems, <http://www.appliedbiosystems.com/>). The thermal cycling program was set as follows: 50 °C for 10 min and 95 °C for 10 min, followed by 40 cycles of 95 °C for 25 s, 58–60 °C for 25 s (optimized for each primer pair), and 72 °C for 30 s, a melting curve stage at 95 °C for 15 s, 60 °C for 1 min, 95 °C for 30 s, and 60 °C for 15 s. If non-specific fluorescence was observed in the melting curve, the reaction was excluded and repeated. Gene-specific primers (Supplementary Table S1 available at *JXB* online) were designed for each of the target genes and for the reference gene (*Actin2*). Samples from each of three biological replicates were assayed in triplicate. Expression values were normalized to those of *Actin2*. The data were then subjected to analysis of variance in a completely randomized design, and the treatment means were separated by Duncan's multiple range test (McNicoll *et al.*, 2006; Nafisi *et al.*, 2007).

ROS level and the lipid peroxidation status

The ROS content of the leaves' response to OTA at 0.1, 0.25, and 1 mM for 24 h was measured as described previously (Peng *et al.*, 2010) and the malondialdehyde (MDA) content was analysed as described previously (Xu *et al.*, 2009).

Measurement of the photosynthetic activity

The photosynthetic activity (Pn) was detected using the LI-6400XT photosynthetic system (LI-COR, Lincoln, NE, USA). The LI-6400XT measures gas exchange over the same leaf area with full control of environmental variables. The concentration of CO₂ was set at 400 µmol mol⁻¹, photosynthetic photon flux density 100 µmol m⁻² s⁻¹, 22 °C, and 60% relative humidity.

Protein extraction and two-dimensional electrophoresis

The extraction of total proteins was performed as described by Chan *et al.* (2007) with some modifications. All procedures described below were carried out at 4 °C. Briefly, 1 g of leaves from 60 single plants were immersed in 70 ml of 0.25 mM OTA in several Petri dishes for 8 h. The extracted protein was solubilized

in 500 µl of lysis buffer containing 7 M urea, 2 M thiourea, 4% (w/v) CHAPS, 1% (w/v) dithiothreitol (DTT; Sigma, <http://www.sigmaaldrich.com/>), 1% (v/v) pH 4–7 IPG buffer, 1% (v/v) pH 3–10 NL IPG buffer (GE Healthcare), and 0.5% (v/v) protease inhibitor cocktail (Sigma-Aldrich). The protein concentration was quantified using a 2-D Quant kit (GE Healthcare) with bovine serum albumin as the standard. The protein samples were stored at –80 °C prior to use.

Two-dimensional electrophoresis (2-DE) of protein extracts was performed using a two-dimensional electrophoresis system (GE Healthcare, <http://www.gehealthcare.com/>), according to the manufacturer's instructions. A 250 µl aliquot of total protein (400 µg) was loaded in 13 cm, pH 3–10 NL IPG strips (GE Healthcare) for isoelectric focusing. Prior to the electrophoresis in the second dimension, the IPG strips were equilibrated by reduction with DTT and carboxymethylation with iodoacetamide. The equilibrated strips were run on 12.5% SDS–polyacrylamide gels at 10 mA per gel for 1 h and 20 mA per gel until the dye front (sealing the IPG Strip gel with agarose sealing solution, containing 0.5% bromophenol blue) reached the bottom end of the gel. Proteins were visualized with Coomassie Brilliant Blue R-250 after 1 h protein fixation in a solution of 50% ethanol, 10% acetic acid, and 40% water. The gels were destained with a solution of 30% ethanol, 8% acetic acid, and 62% water for 2 h and then washed five times with water. Image digitization was carried out with an Image Scanner (GE Healthcare) in transmission mode. Protein expression levels in 2D gel images were compared using the Image Master 2D Elite software (GE Healthcare). To account for experimental variation, at least three gels, resulting from protein extracts obtained from independent experiments, were analysed for each treatment. Statistical analysis of the data was performed using SPSS software, version 11.5 (SPSS Inc., Chicago, IL, USA). The normalized intensity of spots on three replicate 2D gels was averaged, and the standard deviation was calculated for each treatment. A two-tailed unpaired Student's *t*-test was used to determine whether the relative change between control and OTA-treated samples was statistically significant (Chan *et al.*, 2007). Only spots that changed significantly in averaged normalized spot volume were excised for protein identification.

Protein identification

Protein spots with significant changes (at least 2-fold) were carefully cut out from Coomassie Brilliant Blue R-250-stained gels and subjected to in-gel trypsin digestion according to Sun *et al.* (2007) with minor modifications. MALDI-TOF/TOF MS/MS (matrix-assisted laser desorption/ionization-time of flight tandem mass spectrometry) experiments were carried out according to Zhang *et al.* (2006) with minor modifications. GPS Explorer™ software, version 3.6 (Applied Biosystems) was used to create and search files with the MASCOT search program (Matrix Science, <http://www.matrixscience.com/>) for peptide and protein identification. The NCBI Greenplant Database 2009 was used for the search and was restricted to tryptic peptides. Carboxymethylation and oxidation were selected as variable modifications. One missed cleavage was allowed. Precursor error tolerance was set to ~0.2 Da, and MS/MS fragment error tolerance was set to ~0.3 Da. All of the proteins identified had protein scores >61 and individual ion scores >21, with expected *P*-values <0.05. All of the MS/MS spectra were further validated manually.

Digital gene expression: tag profiling (DGE)

Sequence tag preparation was performed with the Illumina Digital Gene Expression Tag Profiling Kit (Illumina, Inc.) according to the manufacturer's protocol. In brief, 6 µg of total RNA was incubated with oligo(dT) magnetic beads to adsorb the polyadenylated RNA fraction. First- and second-strand cDNA was synthesized guided by oligo(dT), and bead-bound cDNA was subsequently digested with *Nla*III to retain a cDNA fragment from

the most 3' CATG to the poly(A) tail. Subsequently, a GEX NlaIII adaptor (adaptor 1) containing a restriction site for *MmeI* was used to cut 17 bp downstream from the *NlaIII* site, thereby releasing 21–22 bp tags starting with the *NlaIII* recognition sequence, CATG. At this point, the fragments detached from the beads and, after dephosphorylation and phenol extraction, a second GEX adaptor (adaptor 2) was ligated at the site of *MmeI* cleavage. After 15 cycles of linear PCR amplification, 85 base strips were purified by 6% TBE PAGE. These strips were then digested, and the single-chain molecules were fixed onto a Solexa Sequencing Chip (flowcell) (Illumina, Inc., <http://www.illumina.com/index.ilmn>). Each molecule grew into a single-molecule cluster sequencing template through amplification. Then four types of nucleotides, labelled with four colours, were added, and sequencing by synthesis (SBS) was performed. Each tunnel generated millions of raw reads with a sequencing length of 35 bp. The raw sequences had 3' adaptor fragments as well as a few low-quality sequences and several types of impurities. The raw sequences were transformed into 17 bp clean tags, and tag counting was carried out using the Illumina Pipeline.

A pre-processed database of all possible CATG+17 nucleotide tags was created using reference gene sequences (ftp://ftp.arabidopsis.org/Sequences/blast_datasets/TAIR9_blastsets/). All clean tags were mapped to the reference sequences, and no more than one nucleotide mismatch was allowed. The clean tags mapped to reference sequences from multiple genes were filtered. The remaining clean tags were designed as unambiguous clean tags. The number of unambiguous clean tags for each gene was calculated and then normalized to the number of transcripts per million clean tags (TPM) using the method described by Hoen *et al.* (2008) and Morrissey *et al.* (2009). Finally, a rigorous algorithm developed by the Beijing Genomics Institute (BGI) referring to 'the significance of digital gene expression profiles' [false discovery rate (FDR) < 0.001] (Audic and Claverie, 1997) was used to identify differentially expressed genes between two samples (Benjamini and Yekutieli, 2001), and absolute value of \log_2 ratio ≥ 1 (minimum of 2-fold difference) as the threshold to judge the significance of gene expression difference.

Statistical analysis

All statistical analyses were performed using Excel 2007 software and SPSS software, version 11.5. The results were considered to be statistically significant at $P < 0.05$. When the analysis was statistically significant, Duncan's multiple range test was applied to the separate mean values.

Results

OTA induces lesion formation in *Arabidopsis* leaves

When an OTA solution (2 mM, 1 mM, or control) was infiltrated into leaves of 4-week-old *Arabidopsis* plants grown in soil in a greenhouse, macroscopic lesions formed on the infiltrated leaves within 1–2 d (Fig. 1A). To determine whether the response of *A. thaliana* to OTA is similar to its response to FB1 and AAL toxin, which both elicit necrotic lesion formation in detached tomato leaves (Stone *et al.*, 2000; Gechev *et al.*, 2004), detached leaves were incubated in Petri dishes containing 0.1 mM, 0.25 mM, or 1 mM OTA. As illustrated in Fig. 1A, macroscopic lesions formed on the leaves exposed to OTA for 3 d. Lesion formation was dose dependent and was evident at concentrations of >0.1 mM OTA. Surrounding the area of necrotic tissue, progressive yellowing of the leaf was clearly visible in the 1 mM and 0.25

mM OTA treatments (Fig. 1B). This yellowing is reflected in a loss of average chlorophyll content as the diameter of the necrotic lesion area increases (Fig. 1C).

Light is required for lesion formation in response to various pathogens (Guo *et al.*, 1995) as well as in some lesion-mimic mutants and in transgenic plants that form spontaneous HR-like lesions (Genoud *et al.*, 1998). As with FB1 (Stone *et al.*, 2000), light is also required for lesion formation in response to OTA. As shown in Fig. 1B, OTA-elicited lesion formation in *Arabidopsis* leaves was greatly reduced in the dark.

The measurement of relative ion leakage was used as an indicator of the extent of cell death; the relative leakage rate in the OTA treatment group was always significantly higher than that in the control group, and the relative leakage rate in the light was higher than that in darkness (Fig. 1D). This showed that leaves of *A. thaliana* were sensitive to OTA, and light could accelerate the process of cell death.

Ultrastructural changes during OTA exposure

Ultrastructural examination of *Arabidopsis* leaves floating in 0.25 mM OTA under continuous light at room temperature (22 °C) revealed very few differences between OTA-treated and methanol-treated controls at 3 h (Fig. 2G), and the cytological damage induced by OTA was first observed at 8 h, prior to chlorophyll reduction. At 8 h, the separation of the plasma membrane from the cell wall, fold formation, chromatin condensation, and the margination and breaking of the nucleolus were observed (Fig. 2A–C). At 24 h, the deformation of cell organelles became more severe, the structures of the mitochondria and chloroplasts were destroyed, the mitochondrial matrix escaped out of the mitochondria, the thickness of the membrane was uneven, part of the nuclear membrane had become invaginated, and some of the nuclei were distorted (Fig. 2D–F). The appearance of control leaves showed changes at 4 d (not shown); however, the obvious destruction of the organelles could be observed at 3 d at the ultrastructural level. Since the condensation of nuclei is an important morphological trait characteristic of apoptosis, the fact that these symptoms were observed in 0.25 mM OTA-treated leaves at 8 h demonstrated that OTA induced cell death in *Arabidopsis* leaves.

Potential of gene expression during OTA exposure

To verify further that a defence response took place and induced cell death under the treatment conditions, 4-week-old *Arabidopsis* leaves were treated with 0.25 mM OTA for 3, 8, and 24 h, and control leaves were treated with 0.122% methanol. Gene expression ratios relative to the control treatment are shown in Fig. 3. Several genes induced by OTA were characterized by potentiated expression of the salicylic acid-inducible marker gene *PR1* and aminocyclopropane carboxylate synthase *ACS6*. These genes were up-regulated as the treatment time increased. The expression of *respiratory burst oxidase homologue C* (*AtrbohC*) and *AtrbohD* increased dramatically after 3 h and 24 h, respectively.

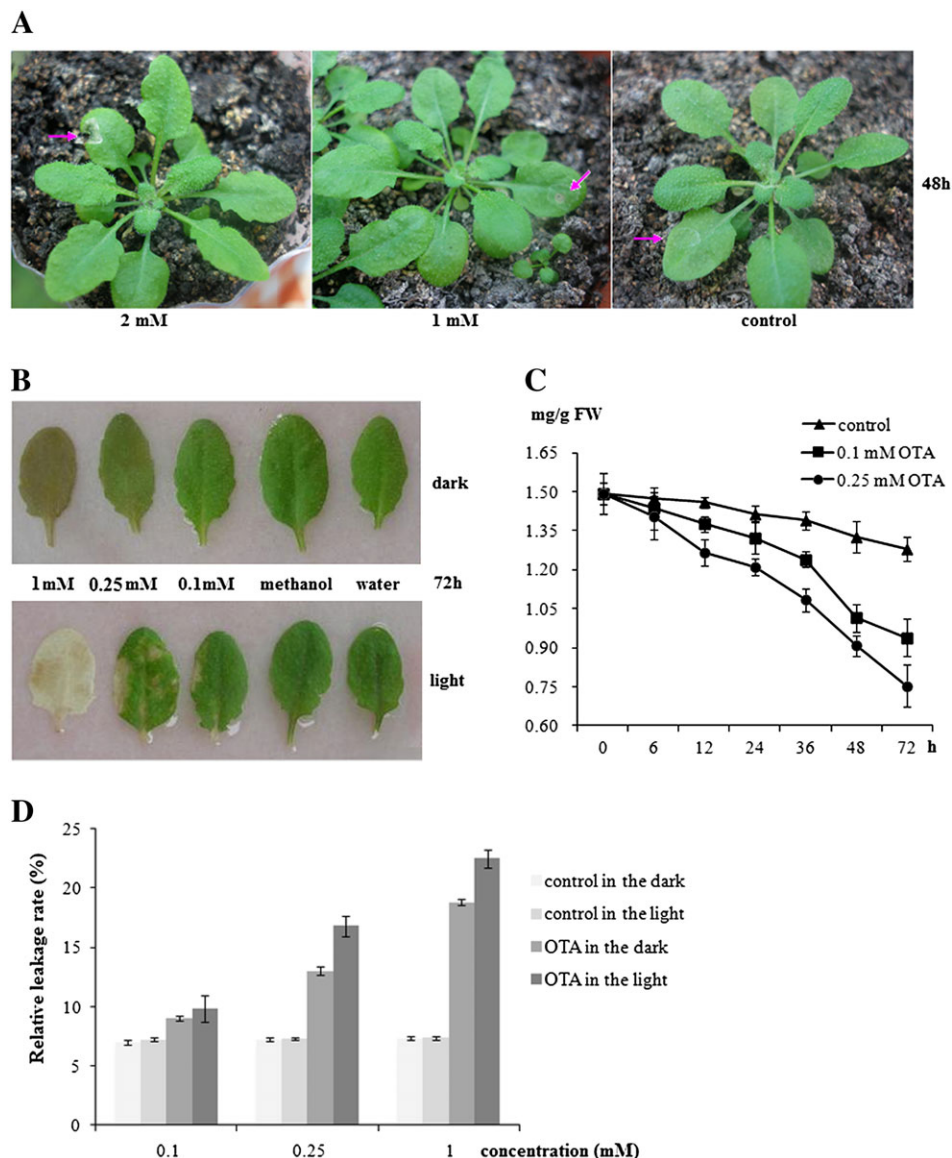


Fig. 1. Development of necrotic lesions and ultrastructural changes during OTA treatment. (A and B) Development of OTA-dependent necrotic lesions in leaves of 4-week-old *Arabidopsis thaliana*. The leaves were infiltrated with a series of OTA concentrations or methanol (control) and photographed at the indicated times. (C) Chlorosis of leaves was observed during the time course after 40 μ M, 0.1 mM, or 0.25 mM OTA treatment; the curve indicates the change in average chlorophyll content relative to the control at time zero. (D) The relative leakage rate in response to OTA at 0.1, 0.25, and 1 mM under dark and light conditions in *Arabidopsis* leaves ($n=3$).

The expression of the *APX* antioxidant gene was in accordance with the ROS level (Fig. 4A). There was a continuous increase in the ROS content with the increase of OTA concentration. The application of OTA to excised *A. thaliana* leaves significantly accelerated the increase in MDA (Fig. 4B).

Proteomic analysis of OTA-induced cell death

Protein samples for 2-DE were obtained from detached leaves after treatment with OTA (Fig. 5). Changes in the abundance of proteins were measured and compared between control and OTA-treated samples in three independent replicates. Analysis of the 2-DE pattern

revealed that most protein spots on the gel had an acidic pI value in the range of pH 4–7 and a molecular mass between 15 kDa and 80 kDa. Approximately 1032–1061 protein spots could be detected on 2D gels after ignoring very faint spots and spots with undefined shapes and areas. Quantitative analysis of spot intensity by integration of the staining signal for each gel and image analysis revealed that the levels of 27 of the resolved proteins changed in an OTA-dependent manner (ratio >1.5) in three independent experiments. The full data set is available in [Supplementary Table S2](#) at JXB online. The spots selected for further analysis are indicated in Fig. 5. Using MALDI-TOF/TOF MS/MS, the 27 protein spots that showed relatively high abundance were analysed. The results of this analysis are summarized

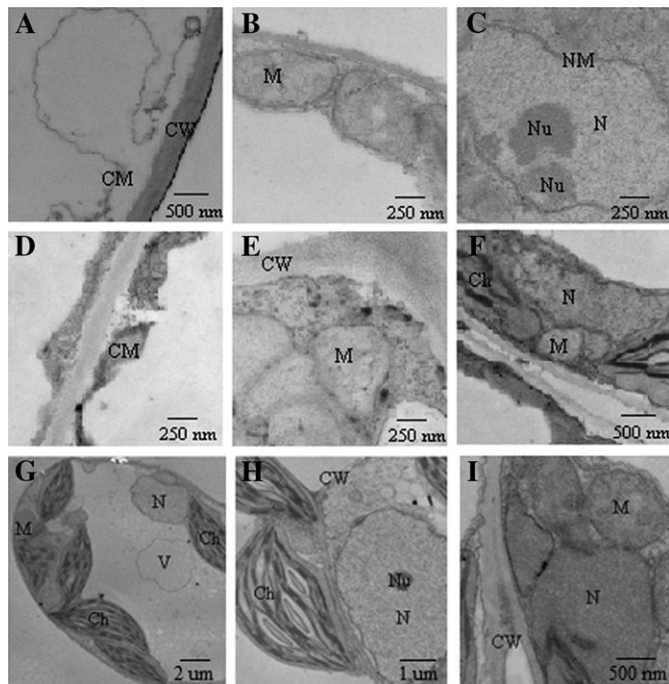


Fig. 2. Ultrastructural changes in the mesophyll cells in *Arabidopsis* leaves induced by OTA. (A–C) Transmission electron micrographs of samples from leaves floating in 0.25 mM OTA for 8 h under continuous light. (A) The separation of plasma membrane from the cell wall and the formation of folds. (B) The membrane of mitochondria became unclear. (C) The agglutination of chromatin and the margination and breaking of the nucleolus. (D–F) Transmission electron micrographs of samples from leaves floating in 0.25 mM OTA for 24 h under continuous light. (D) The thickness of the membrane was uneven, and some membrane sections split. (E) Mitochondria deformed, and the matrix escaped. (F) The nucleus was out of shape. (G–I) Transmission electron micrographs of samples from leaves incubated in an equal volume of methanol for 3, 8, and 24 h under continuous light. CW, cell wall; Ch, chloroplast; M, mitochondria; N, nucleus; NM, nucleus membrane; Nu, nucleolus; V, vacuole.

in Table 1. Four of these differentially expressed proteins (SPs 4, 10, 25, and 27) did not show a total ion score, and the remaining 23 were submitted to the MASCOT search engine for database searching. Among these 23 protein spots, 18, representing 13 different proteins, were identified with significant Mascot scores ($P < 0.05$), whereas five protein spots (SPs 2, 9, 17, 18, and 19) showed relatively low total ion scores.

It is noteworthy that six protein spots (SPs 5, 8, 22, 23, 24, and 26) were identified as the same protein, ribulose biphosphate carboxylase (Rubisco) (Table 1). The location of these spots in the gels differed in molecular mass and pI (Fig. 5), indicating that they might be catabolites of Rubisco or have different post-translational modifications. In total, their expression was increased under OTA stress; the large subunit and small chain of Rubisco were also up-regulated. In addition, seven proteins were identified as enzymes involved in basic metabolism, including transketolase (SP 1), serine hydroxymethyltransferase (SHM1,

SP 3), aminomethyltransferase (SP 6), phosphoribulokinase (PRK, SP 11), sedoheptulose-bisphosphatase (SBPASE, SPs 12), fructose-bisphosphate aldolase (SP 14), and phosphoglycerate kinase (PGK, SP 20). The three transferases (SPs 1, 3, and 6) were all down-regulated, indicating that basic cellular metabolism decreased. PRK, SBPASE, and fructose-bisphosphate aldolase were all up-regulated. These enzymes of the glycolytic pathway and the Calvin cycle catalyse the production of ATP upon exposure to OTA. In addition, a putative RNA-binding protein g5bf (SP 7, 1.6-fold down-regulated), an annexin (AnnAt1, SP 13, 1.8-fold up-regulated), and four photosynthesis-related proteins (SPs 15, 16, 20, and 21) were identified. Although the function of the putative RNA-binding protein is unknown, g5bf was also shown to be differentially expressed in R17 cucumber induced by powdery mildew fungus (Fan *et al.*, 2009); it has been correlated with mycotoxin and fungi stresses.

Transcriptional analysis of OTA-induced cell death

Because changes at the transcript level are not necessarily reflected at the protein level, and to obtain more information about the nature of OTA-triggered cell death, a DGE tag profiling analysis approach was pursued to quantify gene changes in response to OTA. This strategy was based on Illumina high-throughput sequencing technology and the newly assembled *Arabidopsis* reference genome. Samples for DGE analysis were collected 8 h after incubation with 0.25 mM OTA, and the control was treated with 0.122% methanol. The *Arabidopsis* reference genome contains 33 518 genes, and 30 856 (92.06%) of these genes have CATG sites. At the 8 h time point, 197 genes were up- or down-regulated by at least 5-fold, and 3118 (10.11%) genes were up- or down-regulated by at least 2-fold. Of these genes, 1923 showed increased expression, and 1195 showed decreased expression, demonstrating that a massive transcriptional reprogramming took place in the OTA treatment samples compared with the methanol-treated controls. To verify the DGE data, selected genes, including *APX*, *PRI*, and *ACS6* from the DGE analyses, were detected by real-time PCR analysis. Quantification of the signals showed that all the patterns of gene expression were consistent with the DGE results, although the ratios varied to some extent (Fig. 3).

The Gene Ontology (GO) classifications of the most highly regulated genes are shown in Fig. 6. According to the putative homology to sequences present in public databases, the differentially expressed genes were classified into 14 different cellular component categories. Through GO analysis, 164, 337, 519, and 449 genes were found to be differentially expressed in mitochondria (5.3%), the cell nucleus (10.8%), chloroplasts (16.6%), and the plasma membrane (14.4%), respectively. Genes located in these organelles were pivotal and necessary in response to stress, providing defence against mycotoxins. Table 2 shows the genes that were most regulated at each time point and their classification into functional categories including antioxidant metabolism, detoxification of xenobiotics, resistance

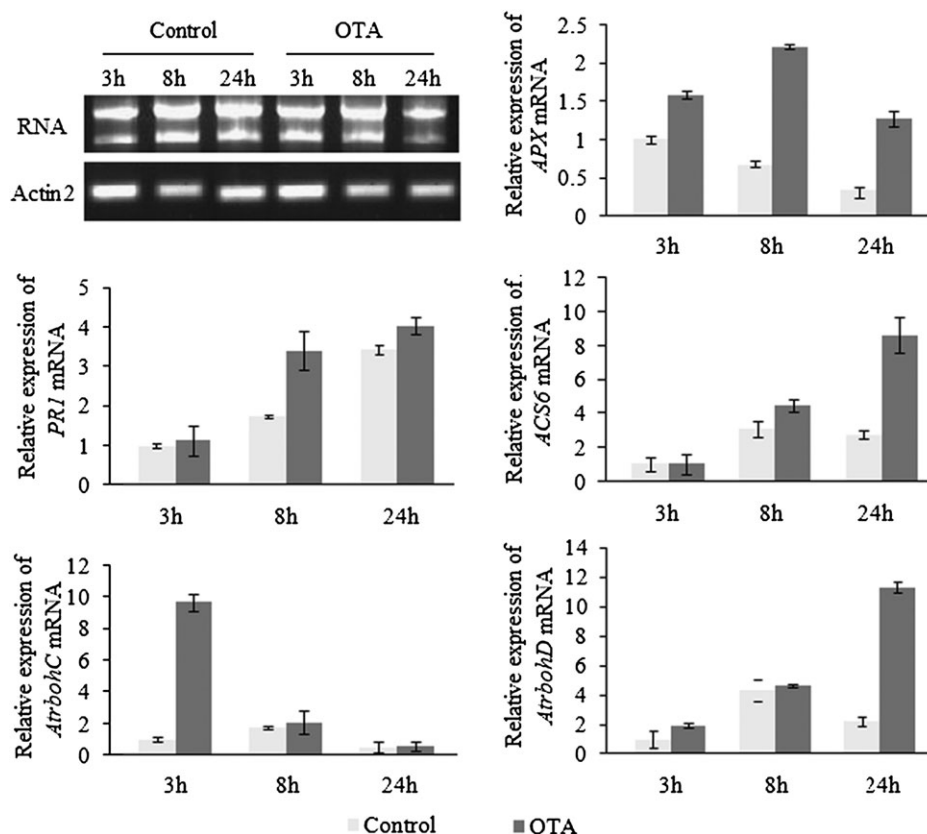


Fig. 3. Real-time PCR analyses of the selected genes, encoding ascorbate peroxidase APX, the salicylic acid-dependent defence-related gene *PR1*, aminocyclopropane carboxylate synthase *ACS6*, *AtrbohC*, *AtrbohD*, and the internal reference gene *Actin2*. Four-week-old *Arabidopsis* leaves were treated with 0.25 mM OTA for 3, 8, and 24 h, and the control was treated with an equal volume of methanol. Samples were harvested after treatment, and gene expression was measured by quantitative RT-PCR. mRNA and *Actin2* were detected by agarose gel electrophoresis, as shown on the left, and relative gene expression ratios (under control treatment) are shown on the right. Standard errors of the mean are shown ($n=3$).

and defence, mitogen-activated protein kinase (MAPK) signalling, transcription factor, hormone signalling, transport, photosynthesis, and the proteasome pathway. The full data set is available in [Supplementary Table S3](#) at *JXB* online.

The DGE data indicated that genes involved in the detoxification of xenobiotics, cytochrome P450 family proteins [including *CYP81D8* (1899), *CYP71A12* (890), *CYP71A22* (504), and *CYP81D1* (202)], UDP-glucuronosyl-transferases (UDPGT) [including *UGT73B4* (8042), *UGT74F1* (347), *UGT88A1* (18.64), *UGT75D1* (13.83), and *UGT75B1* (20.72)], glutathione-*S*-transferases (GST) [including *ATGSTU25* (3383), *ATGSTU2* (1632), *ATGSTU9* (1573), *ATGSTU10* (594), *ATGSTU8* (594), and *ATGSTU12* (415)], as well as ATP-binding cassette (ABC) transporter family members, were dramatically up-regulated. Cytochrome P450 is essential for the primary or phase I metabolism of lipophilic xenobiotics. OTA-inducible *Arabidopsis* cytochrome P450s are homologues of mammalian cytochrome CYP. Biotransformation of many xenobiotics involves UDPGT and GST, which catalyse conjugation reactions (phase II enzymes). OTA is hydrophobic, but conjugates with minor toxicity and high water solubility could be recognized by a glutathione pump, such as ABC and the

ABC transporter, and be transported to the vacuole across the membrane (Taysse *et al.*, 1998). Recently, under certain circumstances, P450s have been shown to produce ROS, resulting in oxidative stress and cell death (Gonzalez, 2005). Xenobiotics were detoxified on a large scale before peak oxidative stress in response to OTA treatment.

Genes such as *FSD1* (2.11), *CAT1* (8.06), *TPX2* (10.68), *GPX6* (4.21), *PRXIIIF* (4.25), *GPX2* (3.17), *GPX3* (2.32), *PER50* (3.85), *PER12* (2.05), *APX3* (4.49), *MDAR2* (2.79), and *MDAR1* (2.54) are up-regulated. These well-known antioxidant genes are considered to be early markers of oxidative stress.

Several regulatory genes, including the transcription factors *WRKY 75* (5876), *AtbZIP15* (445), *AP2 domain-containing transcription factor* (2522), *ANAC 042* (534), *ATHB 8* (504), *WRKY 6* (34.52), *ATMYB102* (621), and *ERF11* (12.48), were up-regulated with OTA treatment. A diverse group of transcription factors are induced early, during the first 8 h of treatment with 0.25 mM OTA: two WRKY family proteins, a zinc finger protein, an AP 2 domain protein, a MYB family member, two NAC domain proteins, and an ERF domain protein are up-regulated. On the other hand, *MAPKKK 19* (504) was the most regulated gene during the MAPK cascade activation process. Activation of

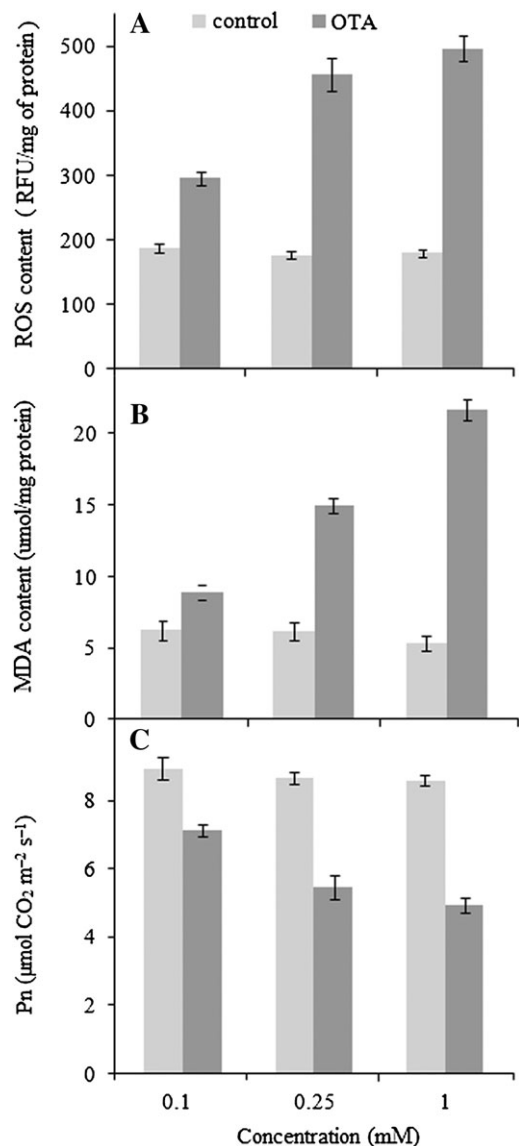


Fig. 4. (A) ROS content measured by H₂DCFDA fluorescence ($n=3$). (B) Lipid peroxidation. MDA content was determined as described in the Materials and methods ($n=3$). (C) The photosynthetic activity (Pn) was detected using the LI-6400XT photosynthetic system ($n=3$). OTA, 0.1 mM, 0.25 mM, 1 mM, Control, an equal volume of methanol.

the MAPK cascade by treatment with OTA was able to dramatically up-regulated the expression of *WRKY 75* (5786), *WRKY 6* (34), and *WRKY 18* (4.8). The changes in the MAPK cascade and transcription factors amplify the signal promptly, protecting the plants against OTA and oxidative stress.

Up-regulation of several elements of the ubiquitin–proteasome pathway, among them the ubiquitin-conjugating enzymes *UBC 3* (39.96) and *UBC 16* (12.58), the UBC13–MMS2 complex (6.15), and many genes from the regulatory and catalytic subunits of the proteasome (Table 2), was observed. The ubiquitin–proteasome system (UPS) targets numerous intracellular regulators. The UPS is not only involved in the degradation of short-lived, damaged, and

misfolded proteins in the cytosol and nucleus during stress and cell death responses, but it also interacts with other components of the cell death machinery, most notably caspases in animal cells or caspase-like proteins in plant cells. In particular, the stress factor UBC 3 participates in all stress responses, playing an important regulatory role (Richard and Vierstra, 2009; Santner and Estelle, 2010).

The pathogenesis-related genes *PR5* (11.1) and *PR1* (17.2), plant defensin *PDF1.2c* (119), and three universal stress proteins (USPs) were strongly up-regulated at the mRNA level during OTA-induced cell death. Repression of the majority of regulated genes and overexpression of two pivotal ethylene biosynthesis genes, *ACS2* and *ACS6*, were also observed (Table 2). The senescence-related gene *SRG2* (71.5) and some senescence-activated genes, including *SAG13* (4.92), *SAG18* (2.40), and *SAG21* (3.41), were overexpressed. Most of the genes implicated in auxin responses to OTA were negatively regulated, just as H₂O₂ can also negatively regulate the auxin responses through activation of the MAPK cascade in *Arabidopsis*. ROS can increase ethylene production through the activation of ACC (1-aminocyclopropane-1-carboxylate) synthase and transcriptional up-regulation of ACC oxidase, two enzymes involved in ethylene biosynthesis. In turn, ethylene can greatly potentiate the oxidative burst (Gechev et al., 2004). In contrast to ROS and ethylene, there was no indication of accumulation of the plant hormones jasmonic acid (JA) and gibberellic acid (GA). Two JA signalling genes, *THI2.2* (–2.75) and *VSP1* (–3.35), were repressed. The thionin genes, arguably the best markers of the presence of JA, were down-regulated. GA2 oxidase 6 (3.45) was up-regulated, but a putative GA-responsive protein (–3.21) was down-regulated, whereas several GA2 oxidases that can degrade GA were up-regulated. Plant hormone signalling is also regulated by ubiquitylation, and the UPS plays an essential role in hormone perception and response (Santner and Estelle, 2010). These signals interact to determine the ultimate fate of the plant cell.

Discussion

Changes in mRNA levels do not always lead to similar alterations in protein levels or enzyme activities. Nevertheless, a comprehensive transcriptome and proteome analysis gives an impression that the dynamics of the cellular processes are involved in the cell death machinery in response to OTA

Photosynthesis and photorespiration

Most of the photosynthesis-related genes that were identified in this study were down-regulated or repressed. Several proteins from both the light reactions (oxygen-evolving enhancer and chlorophyll *a/b*-binding proteins) and dark reactions (Rubisco and Rubisco subunit-binding proteins) of photosynthesis were detected in the proteomic analysis in response to OTA (Fig. 7, Table 1). Photosynthesis provides

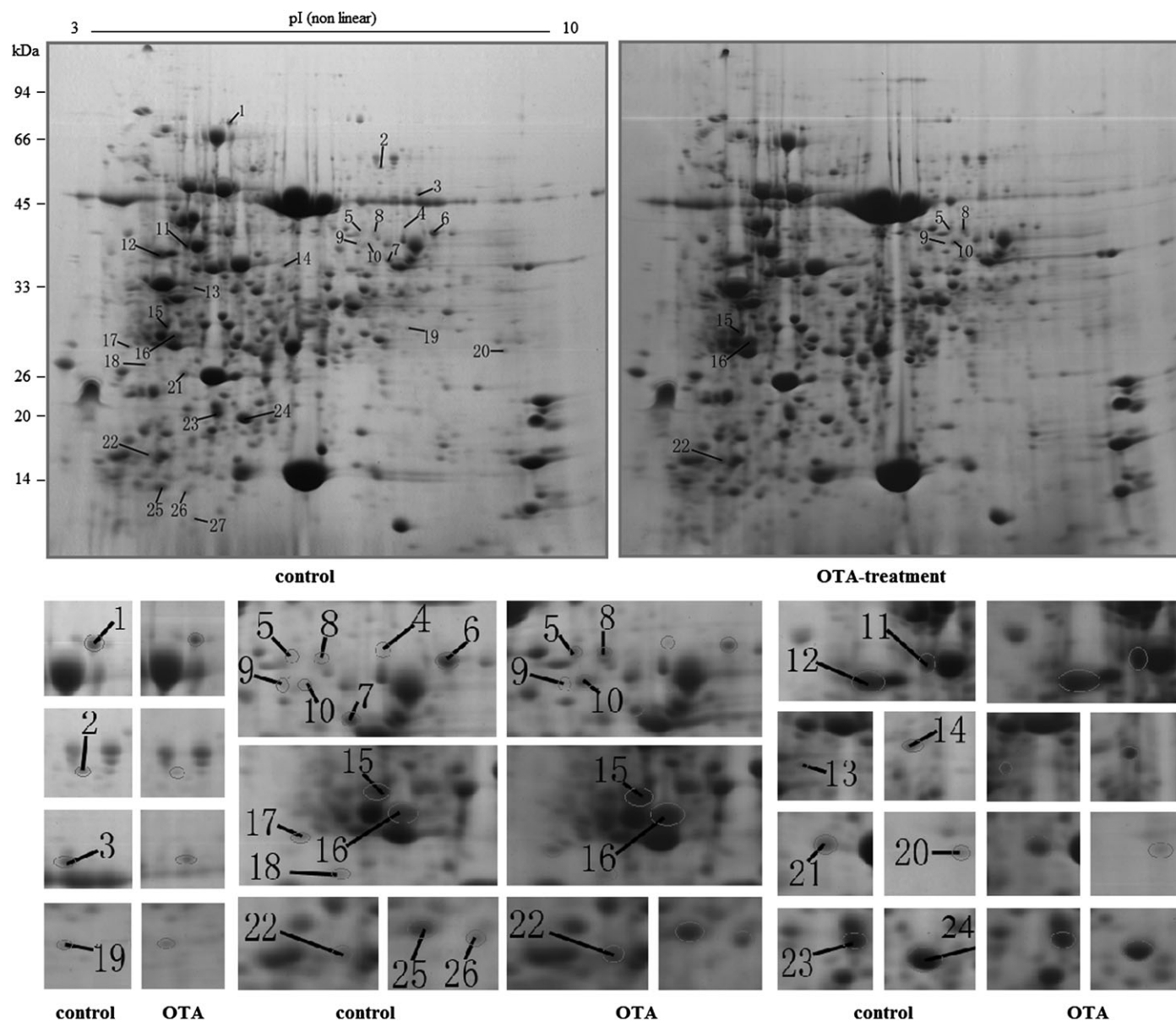


Fig. 5. Images of the 2D gels of total proteins of *Arabidopsis* leaves infected with OTA and methanol (control). *Arabidopsis* leaves were treated with 0.25 mM OTA or methanol solution (control) under continuous light at room temperature (22 °C) for 8 h. Proteins were extracted from *Arabidopsis* leaves with protein extraction buffer by sonication, as described in the Materials and methods. Total protein (400 µg) was separated on 2D gels (pH 3–10 NL) and stained with colloidal Coomassie Brilliant Blue R-250. Arrows indicate proteins that are differentially expressed under OTA stress. The protein spots are numbered, corresponding to the numbers in Table 1. (This figure is available in colour at JXB online.)

oxygen and increases the energy state during the switch to defence and regulation of biosynthetic activities. SP 16, chlorophyll *a/b*-binding protein, was down-regulated (–1.9), coinciding with the gene *CAB* identified in DGE (Fig. 5, Table 2). The essential adjustment factor *CRN1* in the chlorophyll degradation process increased strongly (Fig. 5), and chlorophyllase *ATCLH1* (–5.07) decreased, consistent with the slight chlorosis in leaves and the loss of average chlorophyll content (Fig. 1). The up-regulation of the Rubisco large subunit and small chain indicated that Rubisco was degraded, consistent with reports that Rubisco degradation can be activated by ROS (Liu *et al.*, 2008). The

negative effects of OTA on the large subunits of the three different Rubisco spots (Table 1) revealed that the decrease in Rubisco activity can be explained, in part, by lower Rubisco availability. Photosynthetic activity was reduced (Fig. 4C), which could be associated with the loss of average chlorophyll content and the decrease in Rubisco activity in response to OTA.

Meanwhile, the *SHM1* gene was suppressed, coinciding with its protein expression (Fig. 7, Table 1). *SHM1* encodes the mitochondrial isoform of serine hydroxymethyltransferase (SHMT), which, combined with glycine decarboxylase, catalyses an essential sequence of the C_2 cycle, namely the

Table 1. Identification of intracellular proteins showing differential expression under OTA stress using MS/MS analysis

Spot numbers correspond to those in Fig. 3. Ratio is the average change in abundance expressed as mean intensity \pm SD from three independent treatments; Protein name, matched protein description and the species of the matched protein; NCBI accession no., accession number from the NCBI database of matched proteins; Theo. mol. wt (kDa)/pI, the theoretical molecular mass and isoelectric point based on the amino acid sequence of the identified protein; Exp. mol. wt (kDa)/pI, experimental molecular mass and isoelectric point estimated from the 2D gels; Mascot score/threshold, score obtained from MASCOT for each match and amino acid sequence coverage for the identified proteins; Total ion score, score obtained from MASCOT for all matches; NP, the number of matched peptides; PD, peptides detected.

Spot	Ratio	NCBI accession no. (gi)	Protein name	Mol. wt (kDa) theor./exp.	pI theor./ exp.	Mascot score/ threshold	Total ion score	NP/ PD	Percentage sequence coverage
1	-2.5	gil7329685	Transketolase, putative (<i>Arabidopsis thaliana</i>)	81.9/80	5.80/5.5	383/46	256	5/24	13
3	-1.8	gil15235745	SHM1 (serine hydroxymethyltransferase 1) (<i>Arabidopsis thaliana</i>)	57.4/55	8.13/7.8	266/45	99	7/25	17
5	1.8	gil1944432	Ribulose biphosphate carboxylase (<i>Arabidopsis thaliana</i>)	47.6/46	6.13/6.6	256/47	128	4/20	19
6	-3.7	gil15221119	Aminomethyltransferase, putative (<i>Arabidopsis thaliana</i>)	44.7/45	8.55/8.0	469/44	350	8/19	28
7	-1.6	gil3850621	Putative RNA-binding protein (<i>Arabidopsis thaliana</i>)	42.1/40	7.71/7.5	452/46	358	7/16	21
8	1.7	gil1944432	Ribulose biphosphate carboxylase (<i>Arabidopsis thaliana</i>)	47.6/46	6.13/7.2	382	188	17/24	22
11	1.6	gil15222551	PRK (phosphoribulokinase) (<i>Arabidopsis thaliana</i>)	44.4/44	5.71/5.1	342/46	236	7/17	19
12	1.9	gil15228194	SBPASE (sedoheptulose-bisphosphatase) (<i>Arabidopsis thaliana</i>)	42.4/43	6.17/4.8	519/47	427	10/15	27
13	1.8	gil1429207	AnnAt1 (annexin <i>Arabidopsis</i> 1) (<i>Arabidopsis thaliana</i>)	35.7/35	5.19/5.2	232/46	73	2/20	10
14	1.7	gil15236768	Fructose-bisphosphate aldolase, putative (<i>Arabidopsis thaliana</i>)	38.3/38	5.65/5.8	205/46	110	5/14	20
15	1.5	gil18403751	Plastid-lipid-associated protein PAP (<i>Arabidopsis thaliana</i>)	30.4/30	5.82/4.8	204/46	141	3/10	13
16	-1.9	gil16374	Chlorophyll <i>a/b</i> binding protein (LHCP AB 180) (<i>Arabidopsis thaliana</i>)	25.0/29	5.12/4.9	132/45	75	2/9	23
20	-1.7	gil1022805	PGK (phosphoglycerate kinase) (<i>Arabidopsis thaliana</i>)	41.9/28	4.93/8.7	82/46	40	2/7	9
21	1.6	gil15222166	PSBP-1 (oxygen-evolving enhancer protein 2) (<i>Arabidopsis thaliana</i>)	28.1/26	6.9/5.2	216/46	150	4/11	25
22	1.5	gil7525041	Ribulose bisphosphate carboxylase large subunit (<i>Arabidopsis thaliana</i>)	52.9/18	5.88/4.7	316	237	5/15	11
23	-1.6	gil54306670	Ribulose bisphosphate carboxylase large subunit (<i>Neostenanthera myristicifolia</i>)	52.5/20	6.14/5.5	269/47	205	3/14	7
24	-1.8	gil21555831	Rubisco large subunit (<i>Prostanthera nivea</i>)	28.2/20	8.83/5.6	447/46	388	6/11	27
26	1.6	gil13926229	F1O19.10/F1O19.10 (<i>Arabidopsis thaliana</i>)	14.7/14	5.69/5.2	385/47	307	7/10	52

conversion of two molecules of glycine into one molecule each of CO₂, NH₄⁺, and serine. Photorespiration is caused by the dual affinity of Rubisco for both CO₂ and molecular oxygen, and this cycle involves three organelles (chloroplasts, peroxisomes, and mitochondria) (Voll *et al.*, 2006). Rubisco degradation and loss of SHMT in *Arabidopsis* result in a compromised photorespiratory C₂ cycle and overproduction of ROS, which makes the sample more susceptible to OTA stress (Moreno *et al.*, 2005). This

finding could explain why OTA-elicited lesion formation in *Arabidopsis* leaves was greatly reduced in the dark.

Two kinases related to photosynthesis, PRK (1.6) and PGK (-1.7), participate in photosynthetic carbon dioxide fixation. PRK can catalyse reactions by binding ATP and active Rubisco. PRK was up-regulated, but its gene expression was suppressed at the mRNA level 8 h after OTA treatment. The PGK protein and mRNA levels appeared to be correlated in terms of their expression trends. Oxygen-evolving

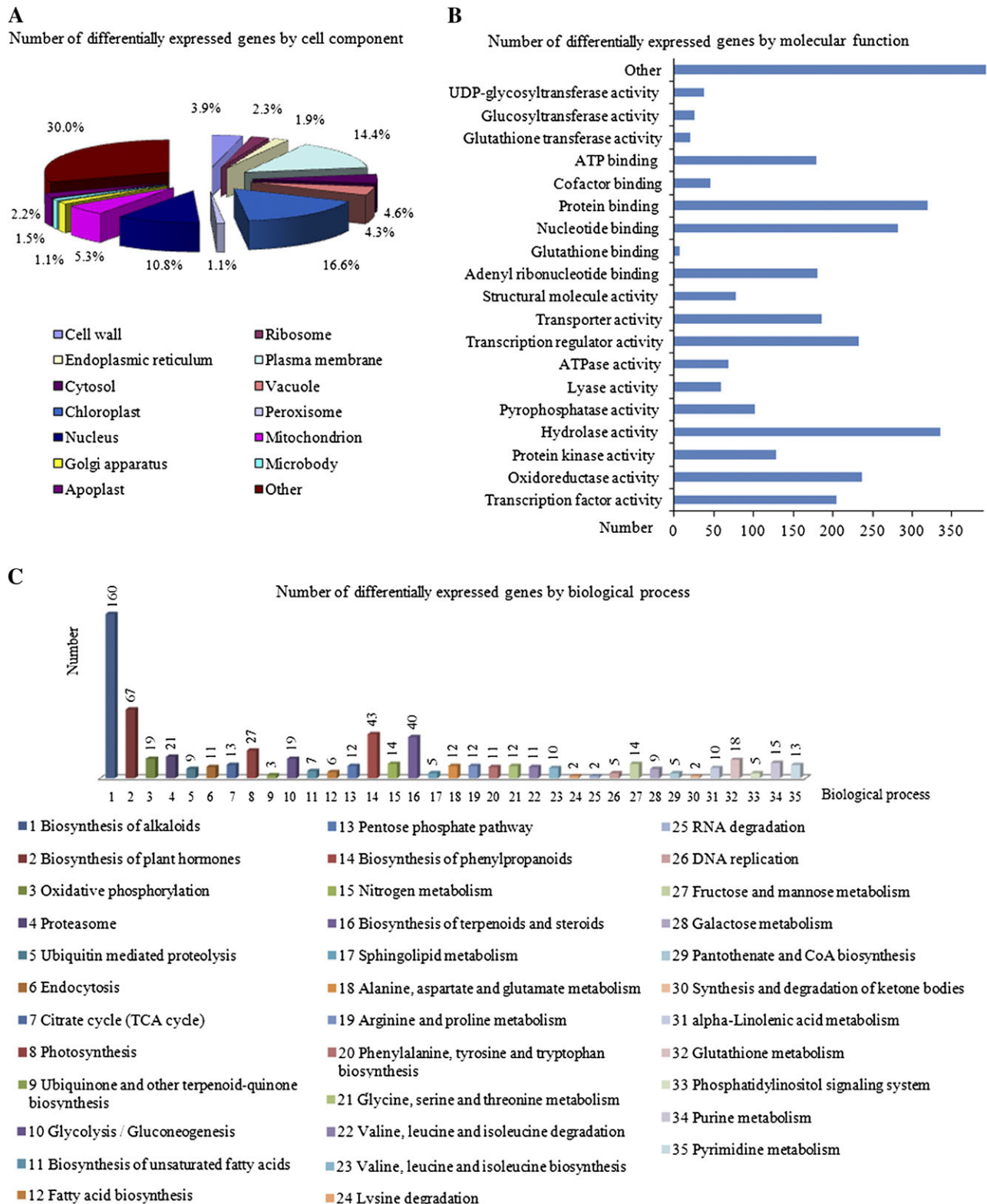


Fig. 6. The most regulated genes were classified by Gene Ontology (GO): cell component (A), molecular function (B), and biological process (C).

enhancer protein 2 of photosystem II (PSII) subunit P PsbP-1 (3.5) was up-regulated at the protein level, but it was simultaneously repressed at the mRNA level. However, PsbP-1 was overexpressed at the mRNA level 3 h after OTA

treatment. The protein level was higher, due to the protein accumulation at the early stage (Fig. 7). In addition, the oxygen-evolving complex (OEC; containing PsbO, PsbP, and PsbQ) is localized on the luminal side of PSII, responsible

Table 2. Global changes in gene expression during OTA-induced cell death

Gene category	Gene	Gene description	Fold change (log ₂)	ID
Antioxidant metabolism	FSD1	Fe superoxide dismutase	2.11 (1.08)	AT4G25100
	CAT1	Catalase	8.06 (3.00)	AT1G20630
	APX3	Ascorbate peroxidase 3	4.49 (2.17)	AT4G35000
	SAPX	Stromal ascorbate peroxidase	2.16 (1.11)	AT4G08390
		Anionic peroxidase, putative	73.12 (6.19)	AT1G14540
		Peroxidase, putative	16.93 (4.08)	AT5G39580
	TPX2	Thioredoxin-dependent peroxidase 2	10.68 (3.42)	AT1G65970
		Peroxidase, putative	4.40 (2.14)	AT4G37530
		Pathogen-responsive alpha-dioxygenase, putative	4.81 (2.26)	AT1G73680
	CM1	Chorismate mutase 1	4.37 (2.13)	AT3G29200
	PRXIIF	Peroxisome oxidoreductase IIF	4.25 (2.09)	AT3G06050
	GPX6	Glutathione peroxidase 6	4.21 (2.08)	AT4G11600
	PER50	Peroxidase 50	3.85 (1.94)	AT4G37520
		Glutathione peroxidase, putative	3.39 (1.76)	AT1G63460
	GPX2	Glutathione peroxidase 2	3.17 (1.67)	AT2G31570
	GPX3	Glutathione peroxidase 3	2.32 (1.21)	AT2G43350
	PER12	Peroxidase 12	2.05 (1.03)	AT1G71695
		Peroxidase, putative	16.93 (4.08)	AT5G39580
	MDAR2	Monodehydroascorbate reductase (NADH)	2.79 (1.48)	AT5G03630
	MDAR1	Monodehydroascorbate reductase, putative	2.54 (1.35)	AT3G52880
	AOX1A	Alternative oxidase	4.51 (2.17)	AT3G22370
	AOX1D	Alternative oxidase	96 (6.59)	AT1G32350
Detoxification of xenobiotics	ATGSTU25	Glutathione S-transferase	3383 (11.72)	AT1G17180
	ATGSTU2	Glutathione S-transferase tau 2	1632 (10.67)	AT2G29480
	ATGSTU9	Glutathione S-transferase	1573 (10.62)	AT5G62480
	ATGSTU10	Glutathione S-transferase	594 (9.21)	AT1G74590
	ATGSTU8	Glutathione S-transferase	564 (9.14)	AT3G09270
	ATGSTU12	Glutathione S-transferase	415 (8.69)	AT1G69920
	ATGSTU11	Glutathione S-transferase	226 (7.82)	AT1G69930
	ATGSTU1	Glutathione S-transferase	152 (7.24)	AT2G29490
	CYP81D8	Cytochrome P450, family 81, subfamily D, polypeptide 8	1899 (10.89)	AT4G37370
	CYP71A12	Cytochrome P450, family 71, subfamily A, polypeptide 12	890 (9.70)	AT2G30750
	CYP71A22	Cytochrome P450, family 71, subfamily A, polypeptide 22	504 (8.98)	AT3G48310
	CYP81D1	Cytochrome P450, family 81, subfamily D, polypeptide 1	202 (7.66)	AT3G28740
		NADP-dependent oxidoreductase, putative	712 (9.48)	AT5G17000
	UGT73B4	UDP-glycosyltransferase 73B4	8042 (12.97)	AT2G15490
	UGT74F1	UDP-glycosyltransferase	347 (8.44)	AT1G05680
	UGT88A1	UDP-glycosyltransferase	18.64 (4.22)	AT2G30140
	UGT75D1	UDP-glycosyltransferase	13.83 (3.79)	AT4G15550
	UGT75B1	UDP-glycosyltransferase	20.72 (4.37)	AT1G05560
	UGT85A1	UDP-glycosyltransferase	13.43 (3.75)	AT1G22400
	ADH1	Alcohol dehydrogenase 1	2.81 (1.49)	AT1G77120
	ADH	Alcohol dehydrogenase, putative	-2.55(-1.35)	AT1G22430
	MDR13	ABC transporter family protein	3.1 (1.62)	AT1G71960
		ABC transporter family protein	2.6 (1.40)	AT1G54350
	ATM1	ABC transporter of the mitochondrion	-4.19(-2.07)	AT4G28630
		ABC transporter family protein	-3.95(-1.98)	AT5G06530
		ABC transporter family protein	-3.87(-1.95)1	AT2G13610
		ABC transporter family protein	-2.07(-1.04)	AT2G01320
Resistance	PR5	Pathogenesis-related gene 5	11.1 (3.48)	AT2G43350
	PR1	Pathogenesis-related gene 1	17.2 (4.11)	AT2G14610
	PDF1.2c	Plant defensin 1.2C	119 (6.89)	AT5G44430
		Immediate-early fungal elicitor family protein	5.39 (2.43)	AT3G02840
	USP	Universal stress protein	7.47 (2.90)	AT3G62550
		Universal stress protein	4.06 (2.02)	AT3G11930
		Universal stress protein	4.48 (2.16)	AT2G47710
	PLP2	Phospholipase 2	9.19 (3.2)	AT2G26560

Table 2. Continued

Gene category	Gene	Gene description	Fold change (log ₂)	ID
MAPK signalling	TSA1	Tryptophan synthase	3.96 (1.99)	AT3G54640
	MAPKKK1	MAP kinase kinase kinase 1	2.97 (1.57)	AT4G08500
	MAPKKK19	MAP kinase kinase kinase 19	504 (8.98)	AT5G67080
	MAPKKK5	MAP kinase kinase kinase 5	3.6 (1.8)	AT5G66850
	MAPKKK10	MAP kinase kinase kinase 10	16.16 (4.01)	AT4G08470
Transcription factor	MAPKKK21	MAP kinase kinase kinase 21	11.92 (3.58)	AT4G36950
	WRKY75	WRKY75 transcription factor	5876 (12.52)	AT5G13080
		AP2 domain-containing transcription factor, putative	2522 (11.30)	AT1G71520
		AP2 domain-containing transcription factor family protein	742 (9.54)	AT2G33710
	ANAC042	<i>Arabidopsis</i> NAC domain-containing protein 42	534 (9.06)	AT2G43000
	ANAC019	<i>Arabidopsis</i> NAC domain-containing protein 19	10.70 (3.42)	AT1G52890
	ATHB8	Homeobox gene 8	504 (8.97)	AT4G32880
	AtbZIP15	bZIP transcription factor family protein	445 (8.80)	AT2G35530
	WRKY6	WRKY6 transcription factor	34.52 (5.11)	AT1G62300
	WRKY18	WRKY18 transcription factor	4.82 (2.27)	AT4G31800
	ATERF	Cooperatively regulated by ethylene and jasmonate 1	15.9 (3.99)	AT3G50260
	ATMYB102	<i>Arabidopsis</i> MYB-like 102	621 (9.28)	AT4G21440
	PIF4	Phytochrome-interacting factor 4	-2.01(-1.00)	AT2G43010
	ERF11	ERF domain protein 11, transcription factor	12.48 (3.64)	AT1G28370
	SZF1	Transcription factor	3.26 (1.71)	AT3G55980
	RAV2	Transcription factor	4.13 (2.04)	AT1G68840
	RHL41	Transcription factor	8.19 (3.03)	AT5G59820
	SAG13	Senescence-activated gene	4.92 (2.30)	AT2G29350
Ageing	SAG21	Senescence-activated gene	3.41 (1.77)	AT4G02380
	SAG18	Senescence-activated gene	2.40 (1.26)	AT1G71190
	SRG2	Senescence-related gene	71.54 (6.16)	AT3G60140
	SRG3	Senescence-related gene	4.32 (2.11)	AT3G02040
	SRG1	Senescence-related gene	3.71 (1.89)	AT1G17020
Ethylene biosynthesis	ACS2	1-Aminocyclopropane-1-carboxylate synthase	5.76 (2.52)	AT1G01480
	ACS6	1-Aminocyclopropane-1-carboxylate synthase 6	4.53 (2.18)	AT4G11280
Jasmonic acid	THI2.2	Thionin 2.2	-2.75(-1.46)	AT5G36910
		Vegetative storage protein-like	-2.20(-1.14)	AT5G44020
	VSP1	Vegetative storage protein 1	-3.35(-1.74)	AT5G24780
Gibberellic acid	GA2OX6	Gibberellin 2-oxidase 6	3.45 (1.79)	AT1G02400
		Gibberellin-responsive protein, putative	-3.21(-1.68)	AT1G22690
Auxin and responses	AXR3	Auxin-resistant 3	-6.43(-2.68)	AT1G04250
		Auxin-responsive family protein	-5.65(-2.50)	AT1G56150
	ARF19	Auxin-responsive factor 19	-3.77(-1.92)	AT1G19220
	AUX1	Auxin-resistant 1	-3.74(-1.91)	AT2G38120
	PIN7	Auxin efflux transmembrane transporter	-3.72(-1.90)	AT1G23080
Photosynthesis	PSAG	Photosystem I subunit G	2.83 (1.50)	AT1G55670
	LHCA1	Chlorophyll binding	5.64 (2.49)	AT3G54890
	LHB1B1	Chlorophyll binding	4.99 (-2.3)	AT2G34430
	LHCB5	Light-harvesting complex of photosystem II 5	-2.14(-1.1)	AT4G10340
	LHCB4.2	Light-harvesting complex PSII	2.11 (1.08)	AT3G08940
	CAB1	Chlorophyll <i>a/b</i> -binding protein 1	-2.62(-1.38)	AT1G29930
	CAB3	Chlorophyll <i>a/b</i> -binding protein 3	-2.68(-1.42)	AT1G29910
	PRK	Phosphoribulokinase	-2.43(-1.28)	AT1G32060
	ATCLH1	Chlorophyllase	-5.07(-2.34)	AT1G19670
	PSB28	Photosystem II reaction centre PSB28 protein	-2.87(-1.52)	AT4G28660
	PsbQ	Oxygen-evolving enhancer 3 (PsbQ)	-2.34(-1.22)	AT1G14150
	PSBTN	Photosystem II subunit T	3.02 (1.59)	AT3G21055
	PSAD-1	Photosystem I subunit D-1	-2.14(-1.10)	AT4G02770
	PSBO-1	PSII oxygen-evolving complex I	-2.05(-1.03)	AT5G66570
	PETE1	Plastocyanin 1	-2.46(-1.29)	AT1G76100
Transporter	TIP2	Tonoplast intrinsic protein 2	-2.74(-1.45)	AT3G26520
	PIP1B	Plasma membrane intrinsic protein 1B	-2.12(-1.08)	AT2G45960

Table 2. Continued

Gene category	Gene	Gene description	Fold change (log ₂)	ID
Proteasome	PIP2E	Plasma membrane intrinsic protein 2E	−2.19(−1.13)	AT2G39010
	PIP1C	Plasma membrane intrinsic protein 1C	−2.73(−1.45)	AT1G01620
	SYP122	Syntaxin of plants 122	3.99 (1.99)	AT3G52400
	SNAP33	SNAP receptor	5.14 (2.36)	AT5G61210
	SYP121	Syntaxin of plants 121	2.42 (1.27)	AT3G11820
	SYP23	Syntaxin of plants 23	−2.83(−1.50)	AT4G17730
	VPS46.2	Vesicle-mediated transport	3.33 (1.74)	AT1G73030
	ATCHX17	Cation/H ⁺ exchanger 17	16.56 (4.05)	AT4G23700
		Sugar transporter, putative	6.81 (2.77)	AT1G08920
		Sugar transporter, putative	4.10 (2.03)	AT3G05165
		Sugar transporter, putative	2.90 (1.54)	AT2G48020
		MATE efflux family protein	415 (8.70)	AT2G04050
		MATE efflux family protein	31.68 (4.99)	AT1G66760
		MATE efflux family protein	10.90 (3.45)	AT3G23550
	PEN3	Penetration 3	2.99 (1.58)	AT1G59870
	VAMP722	Endomembrane-anchored protein	4.11 (2.04)	AT2G33120
	ATS9	Non-ATPase subunit 9	2.7 (1.45)	AT1G29150
	RPN10	Regulatory particle non-ATPase 10	3.0 (1.59)	AT4G38630
	RPN1A	26S proteasome regulatory subunit S2 1A	3.4 (1.78)	AT2G20580
	RPT6A	Regulatory particle triple-A ATPase 6A	3.3 (1.74)	AT5G19990
Ubiquitin	RPT4A	26S proteasome AAA-ATPase subunit RPT4A	3.0 (1.60)	AT5G43010
	RPT5B	26S proteasome AAA-ATPase subunit RPT5B	2.9 (1.53)	AT1G09100
	PAA2	20S proteasome subunit PAA2	4.3 (2.11)	AT2G05840
	PAA1	Proteasome alpha subunit A1	2.7 (1.45)	AT5G35590
	PBC2	Peptidase/threonine-type endopeptidase	5.0 (2.33)	AT1G77440
	PBC1	Proteasome beta subunit C1	4.6 (2.21)	AT1G21720
	PAD1	20S proteasome alpha subunit PDA1	2.2 (1.15)	AT3G51260
	PBE1	Endopeptidase/peptidase/threonine-type endopeptidase	6.6 (2.72)	AT1G13060
	UBC3	Ubiquitin-conjugating enzyme 3	39.96 (5.32)	AT5G62540
	UBC16	Ubiquitin-conjugating enzyme 16	12.58 (3.65)	AT1G75440
	UBC32	Ubiquitin-conjugating enzyme 32	7.66 (2.94)	AT3G17000
	MMZ1	UBC13–MMS2 complex	6.15 (2.62)	AT1G23260
	UBC9	Ubiquitin-conjugating enzyme 9	4.54 (2.18)	AT4G27960
	UBC35	Ubiquitin-conjugating enzyme 35	2.31 (1.21)	AT1G78870
	UBC33	Ubiquitin-conjugating enzyme 33	2.11 (1.08)	AT5G50430

for photosynthetic oxygen evolution; thus, PSII is a target within the photosynthetic apparatus for both biotic and abiotic stress conditions (Pérez-Bueno *et al.*, 2004; Shinya *et al.*, 2010). Previous research showed that *Tobamovirus* infection induced an inhibition of PSII electron transport, disturbing the OEC; the levels of the PsbP and PsbQ extrinsic proteins were lowered to different extents (Pérez-Bueno *et al.*, 2004). In the present experiment, most of the OEC family protein or subunit genes were repressed at the mRNA level (Table 2). OTA treatment specifically induces decreases of OEC family protein; in this sense, damage to OEC activity in OTA-treated plants would intensify photosynthesis disorders.

Transporters and annexin

The regulated transport of molecules across the plasma and vacuolar membranes is a well-characterized response to abiotic stress (Jiang and Deyholos, 2006). Abundant transporters for water, sugars, cations, and other molecules were

detected by DGE in response to OTA (Table 2). The OTA-responsive aquaporins, cation/H⁺ exchanger, and vesicle-mediated transport proteins were also up-regulated transcripts in the present data. Among the remaining antiporters, as well as sugar transporters, ABC, and multi-antimicrobial extrusion (MATE)-like efflux carriers, specific transcripts were induced by OTA treatment (Table 2). Within the MATE family in particular, seven detectable genes were induced >2-fold by OTA, whereas no single MATE gene was equivalently repressed. The large proportion of induced genes within the MATE family, plus the magnitude of their induction, suggests an important role for MATE efflux carriers in the *Arabidopsis* response to OTA. Almost all of the detectable syntaxins of plants were induced by OTA stress in the present data. The *Arabidopsis* syntaxin SYP121 resides in the plasma membrane and forms heterooligomeric complexes for vesicle-mediated secretory defence together with the adaptor SNAP33 and endomembrane-anchored VAMP722. The plasma membrane-resident PEN3 ABC transporter acts in a second pathway and has been implicated

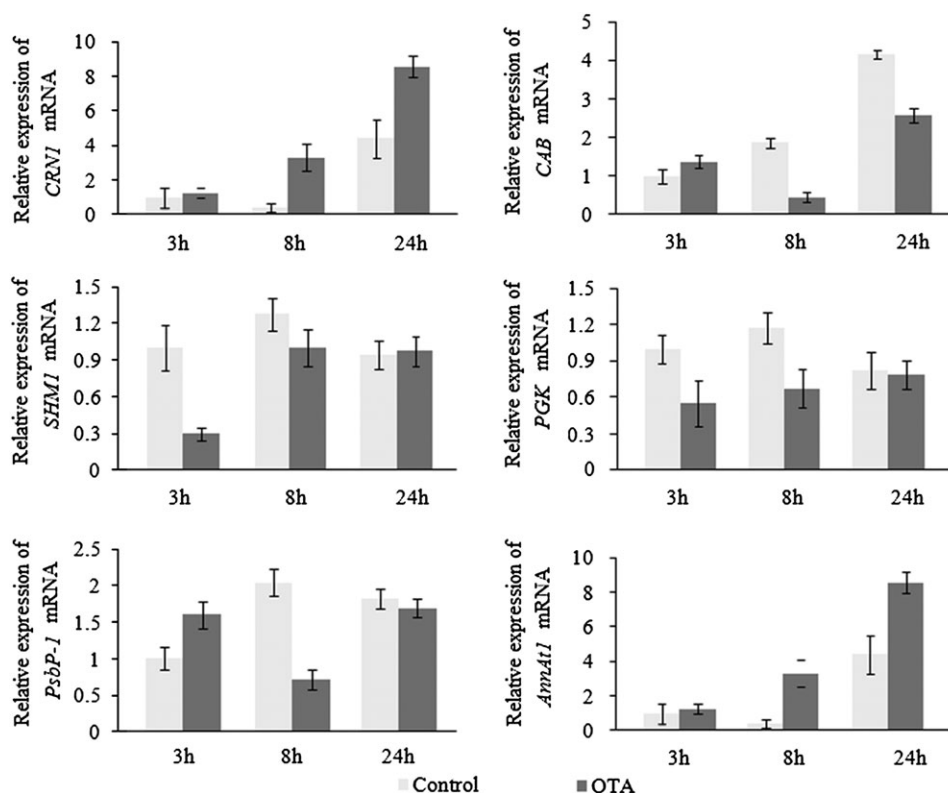


Fig. 7. Real-time PCR analyses of the genes *CRN1*, *CAB*, *SHM1*, *PGK*, *PcbP-1*, *AnnAt1*, and the internal reference gene *Actin2*. Gene expression ratios (relative to the control treatment) are shown. Standard errors of the mean are shown ($n=3$).

in cytoplasmic synthesis, transporting unknown small molecules across the plasma membrane (Bednarek *et al.*, 2009). These results reveal that OTA activates a relatively large transport function of the plasma membrane; in other words, OTA stress signalling is amplified by transmembrane signal transduction.

The annexin *AnnAt1* (1.8) was up-regulated in the proteomic analysis, and its mRNA levels displayed a similar expression trend. The gene encoding *AnnAt1* (AT1G35720) was expressed 1.29-fold under OTA stress (Fig. 7, Table 1). Annexins act as targets of calcium signals in eukaryotic cells, and recent results suggest that they play an important role in plant stress responses. *AnnAt1* mRNA levels were up-regulated in *Arabidopsis* leaves by most of the stress treatments applied (Konopka-Postupolska *et al.*, 2009). Annexins from *Arabidopsis* have peroxidase-like activity, and the expression of some annexins is induced by factors affecting the redox state of the cell. In addition, annexins may contribute to the regulation of ROS levels during the oxidative burst (Gidrol *et al.*, 1996; Gorecka *et al.*, 2005). These experimental data are sufficient to demonstrate that the biological membrane system is a pivotal organelle in response to OTA exposure that senses stress and conducts transmembrane signals. Furthermore, MATE efflux carriers and syntaxin residing in the plasma membrane can transport unknown small molecules across the plasma membrane under OTA stress.

In conclusion, this is the most comprehensive report to date of transcriptomic and proteomic analyses in response

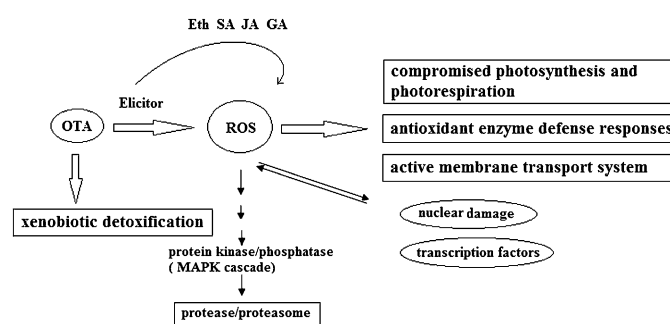


Fig. 8. Hypothetical model of the regulatory network in response to OTA in *Arabidopsis* leaf cells.

to OTA treatment in *Arabidopsis* leaves, and the results showed that OTA induced ROS generation and activated xenobiotic detoxification, plant hormones participated in response to OTA exposure, increased ROS caused antioxidant enzyme defence responses and compromised photosynthesis and photorespiration, and ROS resulted in dynamic changes in transcription factors, nuclear damage, and frequent biological membrane transport as signalling molecules. A hypothetical model of the regulation network activated in response to OTA in *Arabidopsis* leaf cells is shown in Fig. 8. The present study contributes to the understanding of the signalling transduction mechanism that modulates OTA phytotoxicity, facilitates mapping of regulatory networks, and extends the ability to improve OTA tolerance in *Arabidopsis*.

Supplementary data

Supplementary data are available at *JXB* online.

Table S1. Gene-specific primers used to verify the DGE data in real-time PCR analyses. Results of the microarray analysis using ROBIN v. 1.1.5 with standard settings.

Table S2. Protein ratios in response to OTA exposure identified using 2DE and the Independent Samples Test of the SPSS software.

Table S3. Gene Ontology (GO) term enrichment analyses of the digital gene expression profiles.

Acknowledgements

We thank all members of Kunlun Huang's laboratory who contributed to the project, and the Ministry of Science and Technology and the Ministry of Agriculture of China for financial support. We greatly appreciate the help of Researcher Guozheng Qin and Dr Baohua Cao (Institute of Botany, The Chinese Academy of Sciences) in the proteomics experiment.

References

- Anderson JW, Rowan KS.** 1965. Activity of peptidase in tobacco-leaf tissue in relation to senescence. *Biochemical Journal* **97**, 7461–7466.
- Audic S, Claverie JM.** 1997. The significance of digital gene expression profiles. *Genome Research* **7**, 986–995.
- Bednarek P, Piślewska-Bednarek M, Svatoš A, *et al.*** 2009. A glucosinolate metabolism pathway in living plant cells mediates broad-spectrum antifungal defense. *Science* **323**, 101–106.
- Bennett J.** 2003. Mycotoxins. *Clinical Microbiology Reviews* **16**, 497–516.
- Boesch-Saadatmandi C, Loboda A, Jozkowicz A, Huebbe P, Blank R, Wolfram S, Dulak J, Rimbach G.** 2008. Effect of ochratoxin A on redox-regulated transcription factors, antioxidant enzymes and glutathione-S-transferase in cultured kidney tubulus cells. *Food and Chemical Toxicology* **46**, 2665–2671.
- Chan ZL, Qin GZ, Xu X, Li BQ, Tian SP.** 2007. Proteome approach to characterize proteins induced by antagonist yeast and salicylic acid in peach fruit. *Journal of Proteome Research* **6**, 1677–1688.
- Ciacchi-Zanella JR, Jones C.** 1999. Fumonisin B1, a mycotoxin contaminant of cereal grains, and inducer of apoptosis via the tumour necrosis factor pathway and caspase activation. *Food and Chemical Toxicology* **37**, 703–712.
- Egusa M, Ozawa R, Takabayashi J, Otani H, Kodama M.** 2009. The jasmonate signaling pathway in tomato regulates susceptibility to a toxin-dependent necrotrophic pathogen. *Planta* **229**, 965–976.
- Fan HY, Chen J, Shao MN, Xu YF, Zhang CY.** 2009. Proteomic analysis of R17 cucumber differentially expressed proteins induced by powdery mildew fungus. *Acta Horticulturae Sinica* **36**, 829–834.
- Gonzalez FJ.** 2005. Role of cytochromes P450 in chemical toxicity and oxidative stress: studies with CYP2E1. *Mutation Research* **569**, 101–110.
- Gechev TS, Gadjev IZ, Hille J.** 2004. An extensive microarray analysis of AAL-toxin-induced cell death in *Arabidopsis thaliana* brings new insights into the complexity of programmed cell death in plants. *Cellular and Molecular Life Sciences* **61**, 1185–1197.
- Genoud T, Millar AJ, Nishizawa N, Kayb SA, Schäferc E, Nagatanid A, Chua NH.** 1998. An *Arabidopsis* mutant hypersensitive to red and far-red light signals. *The Plant Cell* **10**, 889–904.
- Gidrol X, Sabelli PA, Fern YS, Kush AK.** 1996. Oxygen stress and annexins. *Proceedings of the National Academy of Sciences, USA* **93**, 11268–11273.
- Gorecka KM, Konopka-Postupolska D, Hennig J, Buchet R, Pikula S.** 2005. Peroxidase activity of annexin 1 from *Arabidopsis thaliana*. *Biochemical and Biophysical Research Communications* **336**, 868–875.
- Guo A, Reimers PJ, Leach JE.** 1995. Effect of light on incompatible interactions between *Xanthomonas oryzae* pv. *oryzae* and rice. *Physiological and Molecular Plant Pathology* **42**, 413–425.
- Hoehn PAC, Ariyurek Y, Thygesen HH.** 2008. Deep sequencing-based expression analysis shows major advances in robustness, resolution and inter-lab portability over five microarray platforms. *Nucleic Acids Research* **36**, 141–152.
- Hulten M, Pelser M, Loon LC, Pieterse CMJ, Ton J, Pieterse CMJ, Ton J.** 2006. Costs and benefits of priming for defense in *Arabidopsis*. *Proceedings of the National Academy of Sciences, USA* **45**, 5602–5607.
- Jiang YQ, Deyholos MK.** 2006. Comprehensive transcriptional profiling of NaCl-stressed *Arabidopsis* roots reveals novel classes of responsive genes. *BMC Plant Biology* **6**, 25.
- Konopka-Postupolska D, Clark G, Goch G, Debski J, Floras K, Cantero A, Fijolek B, Roux S, Hennig J.** 2009. The role of annexin 1 in drought stress in *Arabidopsis*. *Plant Physiology* **150**, 1394–1410.
- Lam E, Kato N, Lawton M.** 2001. Programmed cell death, mitochondria and the plant hypersensitive response. *Nature* **411**, 848–853.
- Liu KL, Shen L, Wang JQ, Sheng JP.** 2008. Rapid inactivation of chloroplastic ascorbate peroxidase is responsible for oxidative modification to Rubisco in tomato (*Lycopersicon esculentum*) under cadmium stress. *Journal of Integrative Plant Biology* **50**, 415–426.
- Malekinejad H, Farshid AA, Mirzakhani N.** 2011. Liquorice plant extract reduces ochratoxin A-induced nephrotoxicity in rats. *Experimental and Toxicologic Pathology* **63**, 125–130.
- McNicoll F, Drummelsmith J, Müller M, Boilard N, Ouellette M, Papadopoulou B.** 2006. A combined proteomic and transcriptomic approach to the study of stage differentiation in *Leishmania infantum*. *Proteomics* **6**, 3567–3581.
- Moreno JI, Martin R, Castresana C.** 2005. *Arabidopsis* SHMT1, a serine hydroxymethyltransferase that functions in the photorespiratory pathway influences resistance to biotic and abiotic stress. *The Plant Journal* **41**, 451–463.

- Morrissy AS, Morin RD, Delaney A.** 2009. Next-generation tag sequencing for cancer gene expression profiling. *Genome Research* **19**, 1825–1835.
- Nafisi M, Goregaoker S, Botanga CJ, Glawischnig E, Olsen CE, Halkier BA, Glazebrook J.** 2007. Arabidopsis cytochrome P450 monooxygenase 71A13 catalyzes the conversion of indole-3-acetaldoxime in camalexin synthesis. *The Plant Cell* **19**, 2039–2052.
- Peng XL, Xu WT, Wang Y, Huang KL, Liang ZH, Zhao WW, Luo YB.** 2010. Mycotoxin ochratoxin A-induced cell death and changes in oxidative metabolism of *Arabidopsis thaliana*. *Plant Cell Reports* **29**, 153–161.
- Pérez-Bueno ML, Rahoutei J, Sajjani C, García-Luque I, Barón M.** 2004. Proteomic analysis of the oxygen-evolving complex of photosystem II under biotic stress: studies on *Nicotiana benthamiana* infected with tobamoviruses. *Proteomics* **4**, 418–425.
- Richard D, Vierstra.** 2009. The ubiquitin–26S proteasome system at the nexus of plant biology. *Nature Reviews Molecular cell Biology* **10**, 385–397.
- Ringot D, Chango A, Schneider Y, Larondelle Y.** 2006. Toxicokinetics and toxicodynamics of ochratoxin A, an update. *Chemico-Biological Interactions* **159**, 18–46.
- Santner A, Estelle M.** 2010. The ubiquitin–proteasome system regulates plant hormone signaling. *The Plant Journal* **61**, 1029–1040.
- Shinya Y, Kentaro I, Atsushi T, Seiko I, Kunio I, Noriko I, Tsuyoshi E, Fumihiko S.** 2010. Three PsbQ-like proteins are required for the function of the chloroplast NAD(P)H dehydrogenase complex in *Arabidopsis*. *Plant and Cell Physiology* **51**, 866–876.
- Stone JM, Heard JE, Asai T, Ausubel FM.** 2000. Simulation of fungal-mediated cell death by fumonisinB1 and selection of fumonisin B1-resistant (*fbr*) *Arabidopsis* mutants. *The Plant Cell* **12**, 1811–1822.
- Sun W, Xing BC, Sun YJ, et al.** 2007. Proteome analysis of hepatocellular carcinoma by two-dimensional difference gel electrophoresis. *Molecular and Cellular Proteomics* **6**, 1798–1808.
- Taysse L, Chambras C, Marionnet D, Bosgiraud C, Deschaux P.** 1998. Basal level and induction of cytochrome P450, EROD, UDPGT, and GST activities in carp (*Cyprinus carpio*) immune organs (spleen and head kidney). *Bulletin of Environmental Contamination and Toxicology* **60**, 300–305.
- Voll LM, Jamaï A, Renne P, Voll H, McClung CR, Weber APM.** 2006. The photorespiratory *Arabidopsis shm1* mutant is deficient in *SHM1*. *Plant Physiology* **140**, 59–66.
- Xu WT, Peng XL, Luo YB, Wang JA, Guo X, Huang KL.** 2009. Physiological and biochemical responses of grapefruit seed extract dip on ‘Redglobe’ grape. *LWT-Food Science Technology* **42**, 471–476.
- Zhang X, Boesch-Saadatmandi C, Lou Y, Wolfram S, Huebbe P, Rimbach G.** 2009. Ochratoxin A induces apoptosis in neuronal cells. *Genes Nutrition* **4**, 41–48.
- Zhang XQ, Guo YB, Song YP, et al.** 2006. Proteomic analysis of individual variation in normal livers of human beings using difference gel electrophoresis. *Proteomics* **6**, 5260–5268.